

Angular momentum compensation manipulation to room temperature of the ferrimagnet $\text{Ho}_{3-x}\text{Dy}_x\text{Fe}_5\text{O}_{12}$ detected by the Barnett effect

Masaki Imai,^{1, a)} Hiroyuki Chudo,¹ Masao Ono,¹ Kazuya Harii,¹ Mamoru Matsuo,^{1,2,3} Yuichi Ohnuma,^{2,3} Sadamichi Maekawa,^{1,3,2} and Eiji Saitoh^{1,4,5,6}

¹⁾ *Advanced Science Research Center, Japan Atomic Energy Agency, Tokai 319-1195, Japan*

²⁾ *Kavli Institute for Theoretical Sciences, University of Chinese Academy of Sciences, 19 Yuquan Road, Beijing 100049, P.R.China*

³⁾ *Riken Center for Emergent Matter Science (CEMS), Wako 351-0198, Japan*

⁴⁾ *Advanced Institute for Materials Research, Tohoku University, Sendai 980-8577, Japan*

⁵⁾ *Institute for Materials Research, Tohoku University, Sendai 980-8577, Japan*

⁶⁾ *Department of Applied Physics, The University of Tokyo, Hongo, Bunkyo-ku, Tokyo, 113-8656, Japan*

(Dated: 10 April 2019)

We demonstrate that the angular momentum compensation temperature T_A , at which the net angular momentum in the sample disappears, can be controlled in $\text{Ho}_3\text{Fe}_5\text{O}_{12}$ by partially substituting Dy for Ho. The T_A can be detected using the Barnett effect, by which mechanical rotation magnetizes an object due to spin-rotation coupling. We found that T_A increases with the Dy content and clarified that the T_A of $\text{Ho}_{1.5}\text{Dy}_{1.5}\text{Fe}_5\text{O}_{12}$ coincides with room temperature. The Barnett effect enables us to explore materials applicable to magnetic devices utilizing the angular momentum compensation only by rotating the powder sample at room temperature.

Angular momentum compensation is a key characteristic in the field of spintronics, where attention is focused on the high-speed magnetic response at the angular momentum compensation temperature.¹⁻⁴ N-type ferrimagnets have a magnetic compensation temperature T_M , at which magnetization disappears even in the ferrimagnetically ordered state. Furthermore, when g -factors of the magnetic moment belonging to different sublattices are different, the ferrimagnetic materials have an additional compensation, namely the angular momentum compensation temperature T_A , at which the net angular momentum $\langle J_{\text{net}} \rangle$ in the material disappears even in the magnetically ordered state. While T_M is easily determined by magnetization measurements, T_A cannot be determined by conventional magnetization measurements using a magnetic field. It was recently reported that the domain wall mobility was enhanced at T_A in GdFeCo .⁴ However, this method requires microfabrication of materials and only applies to metals. Nevertheless, using the Barnett effect, a phenomenon by which a rotating object is magnetized by spin-rotation coupling, the angular momentum compensation can be determined.⁵

The Barnett effect was discovered in 1915.^{6,7} The angular momentum of electrons in matter interacts with rotational motion through spin-rotation coupling, described as

$$\mathcal{H} = -\mathbf{J} \cdot \boldsymbol{\Omega}, \quad (1)$$

where \mathbf{J} is the angular momentum and $\boldsymbol{\Omega}$ is the angular velocity.⁸ The angular momentum is then aligned with

the direction of the rotation axis, which causing magnetization. With ferrimagnets, \mathbf{J} is represented as the sum of the angular momenta belonging to different sublattices $\langle J_{\text{net}} \rangle$. The Barnett effect does not apply when $\langle J_{\text{net}} \rangle = 0$, which is the definition of the angular momentum compensation.

In this letter, we demonstrate T_A control for the insulating rare earth iron garnet $\text{Ho}_{3-x}\text{Dy}_x\text{Fe}_5\text{O}_{12}$. T_A is observed using the Barnett effect.⁵ To realize a high-speed magnetic device using the angular momentum compensation, T_A should coincide with the temperature at which the device is operated. We found that T_A coincides with room temperature (20°C) at $x = 1.5$.

Powder samples of $\text{Ho}_{3-x}\text{Dy}_x\text{Fe}_5\text{O}_{12}$ were prepared from Fe_2O_3 (4N), Ho_2O_3 (3N), and Dy_2O_3 (3N) via a solid-state reaction. Fe_2O_3 , Ho_2O_3 , and Dy_2O_3 powders were mixed in a molar ratio of 5 : 3 - x : x in an agate mortar. The mixed powder was pelletized and heated to 1200 °C–1400 °C in the ambient atmosphere. To characterize the samples, the DC-magnetization measurements were performed by extraction magnetometry with a commercial magnetometer (PPMS, Quantum Design).

Figure 1(a) shows the temperature dependence of the magnetization of $\text{Ho}_{3-x}\text{Dy}_x\text{Fe}_5\text{O}_{12}$. The magnetization of both the end materials, $\text{Ho}_3\text{Fe}_5\text{O}_{12}$ (HoIG) and $\text{Dy}_3\text{Fe}_5\text{O}_{12}$ (DyIG), vanishes at $T_M = 135$ and 218 K, respectively. For the substituted materials, the magnetization does not disappear completely due to the T_M distribution; thus T_M was defined as the temperature at which the magnetization shows a local minimum. Figure 1(b) shows the linear relation between T_M and the Dy concentration, and a schematic of the magnetization at sublattices. In the high-temperature region above T_M ,

^{a)}Electronic mail: imai.masaki@jaea.go.jp

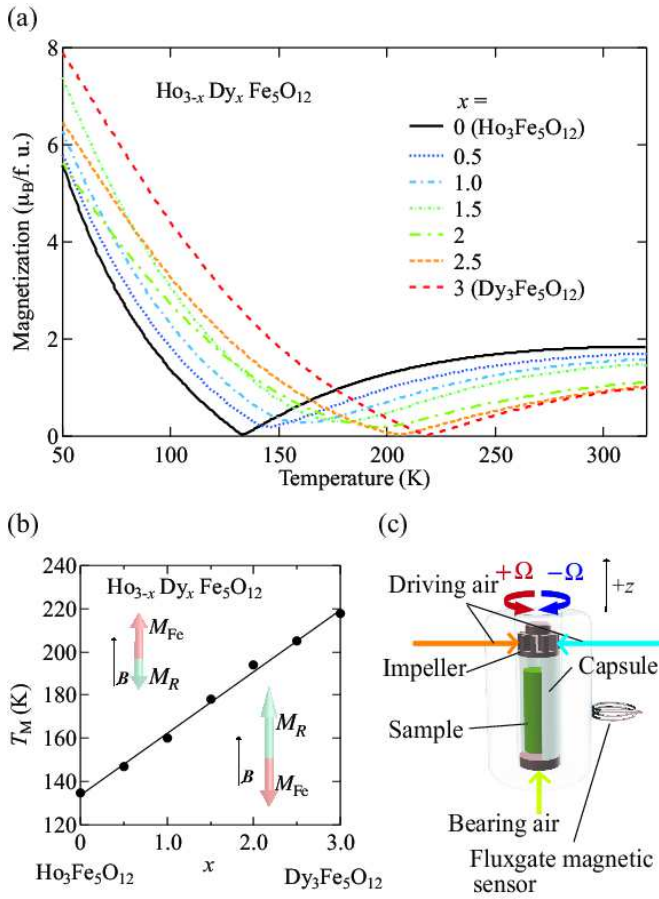


FIG. 1. (a) Temperature dependence of $\text{Ho}_{3-x}\text{Dy}_x\text{Fe}_5\text{O}_{12}$ magnetization in a magnetic field of 1,000 Oe. (b) The variation in magnetization compensation temperature T_M with the Dy content x in $\text{Ho}_{3-x}\text{Dy}_x\text{Fe}_5\text{O}_{12}$. (c) Schematic of the apparatus for Barnett effect measurement using an air-driven rotor system.

since the magnetization at the Fe^{3+} sublattice, M_{Fe} , is larger than that at the R^{3+} sublattice, M_R , M_{Fe} aligns parallel to the magnetic field. The magnitude of M_R increases as the temperature decreases, and M_R equals M_{Fe} at T_M . The magnetization of these sublattices flips across T_M , and then M_R aligns parallel to the magnetic field below T_M (see Section I of Supplementary Material for more details).

We measured the Barnett effect to observe angular momentum compensation. Our apparatus for rotating samples uses an air-driven rotor system as shown in Fig. 1(c).^{5,9-11} The rotor system was placed in magnetic shields to exclude the geomagnetic field. The sample was rotated using compressed air with angular velocity Ω and magnetized to M_Ω by the rotation. We measured the stray field from M_Ω using a fluxgate magnetic sensor. To remove the residual background magnetic field, we measured the difference in the stray field $\Delta B = [B(+\Omega) - B(-\Omega)]/2$, where $B(+\Omega)$ and $B(-\Omega)$ represent the stray fields obtained at $+\Omega$ and $-\Omega$, re-

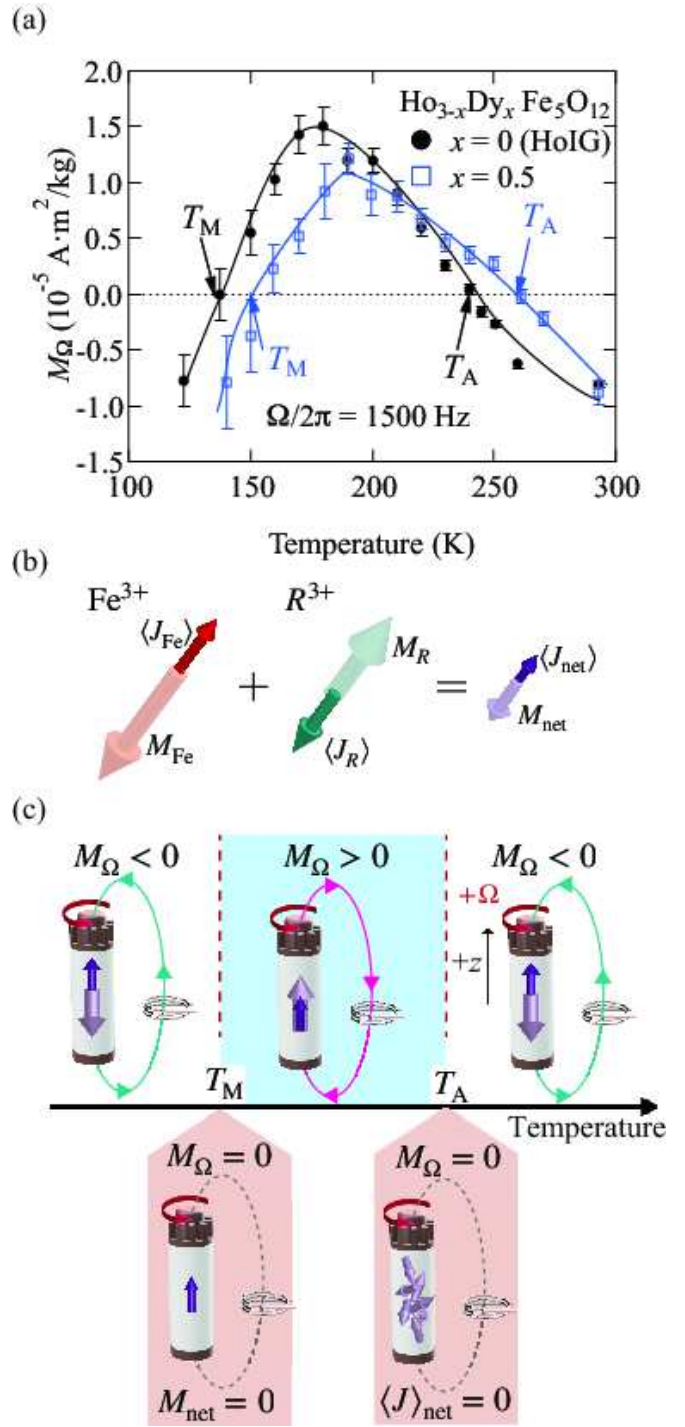


FIG. 2. (a) Temperature dependence of M_Ω of $\text{Ho}_{3-x}\text{Dy}_x\text{Fe}_5\text{O}_{12}$ ($x = 0$ and 0.5). The solid lines are the guide for eyes. (b) Schematic illustration of angular momentum and magnetic moment. Relationship between angular momentum (dark red and blue arrows) and magnetic moment (light red and blue arrows) in $\text{Ho}_{3-x}\text{Dy}_x\text{Fe}_5\text{O}_{12}$. (c) Relationship between angular momentum and the magnetization M_Ω induced by rotation at various temperature. The dark and light purple arrows show net angular momentum and magnetization of $\text{Ho}_{3-x}\text{Dy}_x\text{Fe}_5\text{O}_{12}$, respectively.

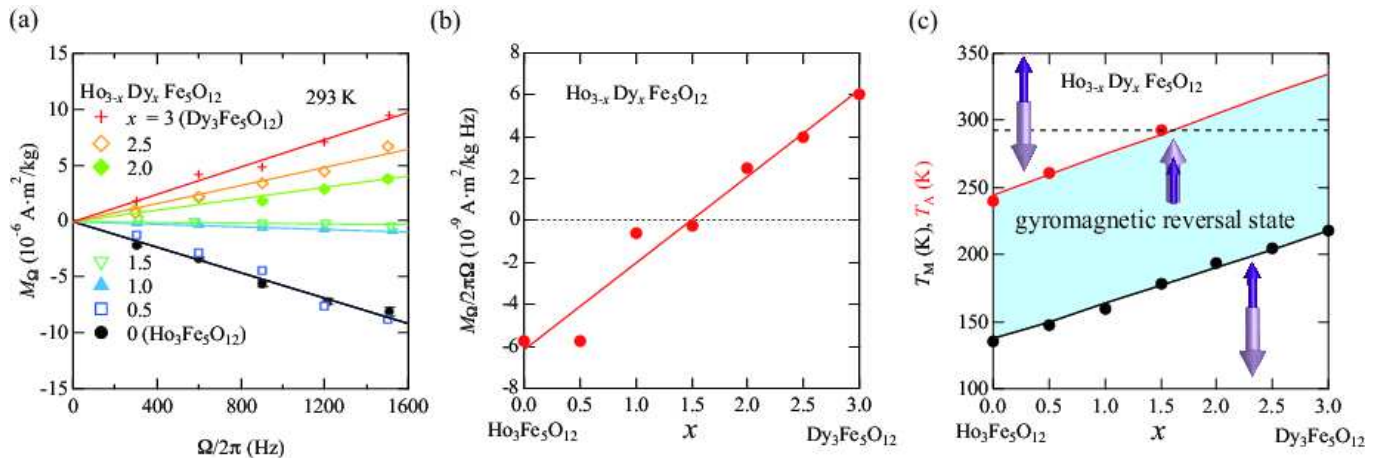


FIG. 3. (a) Rotational frequency dependence of M_Ω for $x = 0, 0.5, 1.0, 1.5, 2.0, 2.5$ and 3.0 at 293 K. (b) Dy content x dependence of the rotation-susceptibility $M_\Omega/2\pi\Omega$ at 293 K. (c) Phase diagram of $\text{Ho}_{3-x}\text{Dy}_x\text{Fe}_5\text{O}_{12}$. Black and red circles indicate T_M and T_A , respectively. Black line is the linear fit to the T_M data. Red line is the calculated T_A (see Section III of Supplementary Material). The blue area represents the gyromagnetic reversal region, where the directions of the net angular momentum and net magnetic moment are aligned in parallel.

spectively (Fig. 1(c)). The measurements were repeated over 20 times to remove fluctuation of the background magnetic field and increase data accuracy. M_Ω was calculated from ΔB using the dipole model described in Ref. 10. For experimental details of Barnett effect measurement at room temperature and low temperatures, see Refs. 10 and 5, respectively.

Figure 2(a) shows the temperature dependence of M_Ω of the Dy content for $x = 0$ and 0.5 at a rotational frequency of $\Omega/2\pi = 1.5$ kHz. The M_Ω of HoIG crosses zero at two temperatures, $T_M = 135$ K and $T_A = 240$ K.⁵ On Dy substitution with $x = 0.5$, T_M and T_A increase to 150 and 260 K, respectively. This indicates that Dy substitution in HoIG can control T_M and T_A .

In $\text{Ho}_{3-x}\text{Dy}_x\text{Fe}_5\text{O}_{12}$, the net angular momentum $\langle J_{\text{net}} \rangle$ and magnetization M_{net} are described as $\langle J_{\text{net}} \rangle = \langle J_{\text{Fe}} \rangle - \langle J_R \rangle$ and $M_{\text{net}} = M_{\text{Fe}} - M_R$, where $\langle J_{\text{Fe}} \rangle$ ($\langle J_R \rangle$) and M_{Fe} (M_R) represent the expected angular momentum and magnetization at Fe^{3+} (R^{3+}) sublattices, respectively (Fig. 2(b)). An effective g factor is defined as $M_{\text{net}} = g\langle J_{\text{net}} \rangle$.

Above T_A , since $\langle J_{\text{net}} \rangle$ and M_{net} are coupled antiparallel due to the negative sign of the effective g factor, M_Ω becomes negative as shown in Fig. 2(c), because Eq. (1) indicates that $+\Omega$ rotation aligns $\langle J_{\text{net}} \rangle$ with the $+z$ direction. At T_A , since the Barnett effect does not apply due to the net zero angular momentum, M_Ω becomes zero. In the range of temperatures between T_A and T_M , M_Ω becomes positive. This indicates that $\langle J_{\text{net}} \rangle$ and M_{net} are coupled parallel; the sign of the g factor becomes positive: this is a gyromagnetic reversal state.⁵ At T_M , though $\langle J_{\text{net}} \rangle$ aligns with the rotation axis, M_Ω is zero due to disappearance of M_{net} at T_M . Below T_M , M_Ω becomes negative again due to the antiparallel coupling between $\langle J_{\text{net}} \rangle$ and M_{net} . The increase in T_A with increasing x indicates that T_A coincide with room tem-

perature (293 K) at appropriate Dy substitution.

To investigate the $\text{Ho}_{3-x}\text{Dy}_x\text{Fe}_5\text{O}_{12}$ composition with $T_A = 293$ K, the rotational frequency dependence of M_Ω was measured for various $\text{Ho}_{3-x}\text{Dy}_x\text{Fe}_5\text{O}_{12}$ compositions at 293 K as shown in Fig. 3(a). For all compositions, M_Ω is proportional to Ω , indicating that the Barnett effect was correctly measured. In HoIG, M_Ω is negative and decreases as Ω increases because $\langle J_{\text{net}} \rangle$ and M_{net} are coupled antiparallel above $T_A = 240$ K (see Fig. 2(a)). As the Dy content x increases, the slope of M_Ω vs. Ω gradually increases, becoming almost 0 at $x = 1.5$, and becoming positive at $x \geq 2.0$. Figure 3(b) shows the initial susceptibility induced by rotation: $M_\Omega/2\pi\Omega$ at 293 K. $M_\Omega/2\pi\Omega$ increases with increasing Dy content x . From the linear fit to the data, T_A is equal to 293 K at $x = 1.49 \pm 0.31$.

Figure 3(c) shows a phase diagram of $\text{Ho}_{3-x}\text{Dy}_x\text{Fe}_5\text{O}_{12}$. Both T_M and T_A depend linearly on x . The black line is the linear fit to the T_M data. The red line is obtained by calculating the temperature dependence of $\langle J_R \rangle$ with various Dy contents (see Sections II and III of Supplementary Material). The calculations are consistent with our experimental results.

Here, we consider the Dy substitution effect on T_M . In the general rare earth iron garnet (RIG) system, T_M predominantly depends on M_R , which contains two factors: the size of the R^{3+} magnetic moment $\mu = -gJ$, and $R^{3+}\text{Fe}^{3+}$ interaction (see Section I of Supplementary Material). Since the Néel temperature is almost irrelevant to the rare earth R^{3+} , the ferrimagnetic order in RIG is predominantly contributed by the $\text{Fe}^{3+}\text{Fe}^{3+}$ interaction. Thus, the temperature dependence of magnetization at the Fe^{3+} sublattice can be regarded as almost the same in the RIG series. The $R^{3+}\text{Fe}^{3+}$ interaction contributes to the temperature dependence of the magnetization at R^{3+} sublattice. The $R^{3+}R^{3+}$ interaction is much weaker than

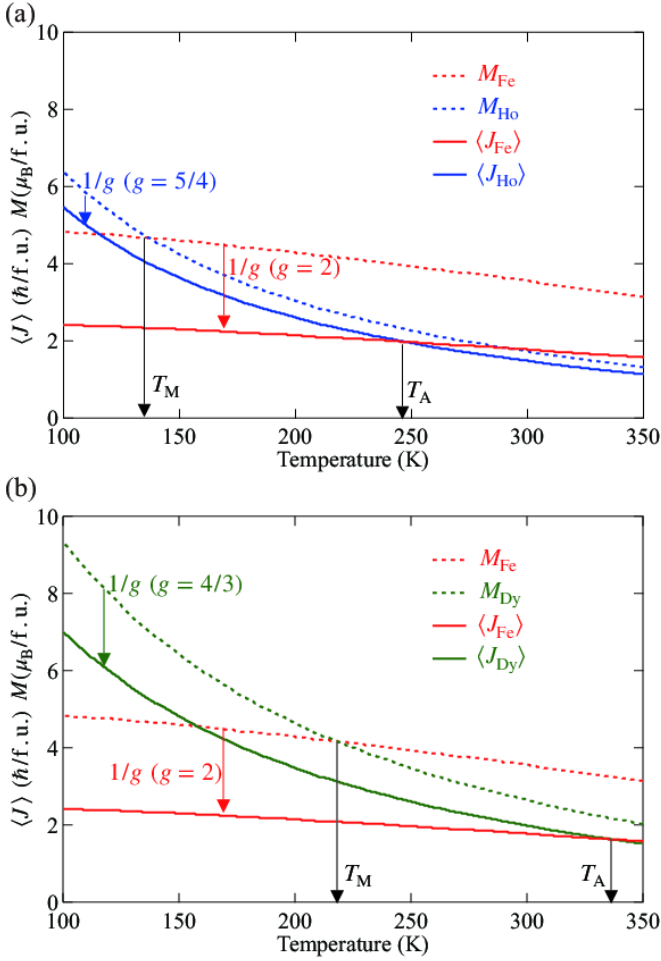


FIG. 4. Temperature dependence of angular momenta and magnetic moments of sublattice magnetic ions in $\text{Ho}_3\text{Fe}_5\text{O}_{12}$ (a) and $\text{Dy}_3\text{Fe}_5\text{O}_{12}$ (b). Red, blue, and green dashed lines indicate the magnetic moments of Fe, Ho, and Dy sites, respectively. Solid lines indicate the angular momenta.

any other interactions in RIG and is negligible except in the very low temperature region. With HoIG and DyIG, since Ho^{3+} and Dy^{3+} have the same magnetic moment of $\mu = 10 \mu_B$, T_M only depends on the $R^{3+}\text{Fe}^{3+}$ interaction. Figure 4 shows the calculated temperature dependence of sublattice magnetization (see Section II of Supplementary Material). Because of the stronger $\text{Dy}^{3+}\text{Fe}^{3+}$ interaction compared to $\text{Ho}^{3+}\text{Fe}^{3+}$, the magnetization at the Dy^{3+} sublattice is larger than that at the Ho^{3+} sublattice. Consequently, the T_M of DyIG is higher than that of HoIG.

In contrast to T_M , T_A depends on $\langle J_R \rangle$, which contains two factors: the size of the R^{3+} angular momentum J_R , and the $R^{3+}\text{Fe}^{3+}$ interaction. The calculated temperature dependence of the angular momenta at the Ho^{3+} and Dy^{3+} sublattices is shown in Fig. 4. Although the angular momentum of Dy^{3+} ($J_{\text{Dy}} = 15/2$) is smaller than that of Ho^{3+} ($J_{\text{Ho}} = 8$), $\langle J_{\text{Dy}} \rangle$ is larger than $\langle J_{\text{Ho}} \rangle$ because the $\text{Dy}^{3+}\text{Fe}^{3+}$ interaction is stronger than the $\text{Ho}^{3+}\text{Fe}^{3+}$ in-

teraction. Therefore, the T_A of DyIG is larger than that of HoIG.

We now discuss the relative values of T_M and T_A . Essentially, the difference between T_M and T_A originates in the difference in the g factors of the ions belonging to different sublattices. Especially, when all the ions have the same g factor, T_A merges with T_M . When the difference in g factors between Fe^{3+} and R^{3+} increases, so does the difference between T_M and T_A . In the $\text{Ho}_{3-x}\text{Dy}_x\text{Fe}_5\text{O}_{12}$ system, the g factors of Fe^{3+} , Ho^{3+} , and Dy^{3+} are 2, 5/4, and 4/3, respectively. Since the difference in the g factors in DyIG is smaller than that in HoIG, the difference between T_M and T_A is expected to be smaller in DyIG than in HoIG. However, the experimental result shows that $T_A(x)$ increases at almost the same rate as $T_M(x)$ against temperature as shown in Fig.3(c). This is due to competition between two effects of Dy substitution: T_A increases due to the stronger $\text{Dy}^{3+}\text{Fe}^{3+}$ interaction compared to $\text{Ho}^{3+}\text{Fe}^{3+}$, and T_A decreases relative to T_M due to the larger g factor of Dy^{3+} compared to that of Ho^{3+} .

In summary, we controlled the angular momentum compensation temperature of $\text{Ho}_{3-x}\text{Dy}_x\text{Fe}_5\text{O}_{12}$ by Dy substitution, and found that T_A coincides with room temperature at $x = 1.5$ in this system using our apparatus for measuring the Barnett effect. Using the Barnett effect, T_A is easily obtained without microfabrication of the sample, regardless of the metal or insulator. The Barnett effect enables us to explore candidate materials for high-speed magnetic devices exploiting fast-magnetization reversal at angular momentum compensation.

SUPPLEMENTARY MATERIAL

See supplementary material for details of the magnetic structure of the samples and their calculated magnetization and angular momentum.

ACKNOWLEDGMENTS

This work was supported by JST ERATO Grant Number JPMJER1402, JSPS Grant-in-Aid for Scientific Research on Innovative Areas Grant Number JP26103005, and JSPS KAKENHI Grant Numbers JP16H04023, JP17H02927.

¹M. Binder, A. Weber, O. Mosendz, G. Woltersdorf, M. Izquierdo, I. Neudecker, J. R. Dahn, T. D. Hatchard, J.-U. Thiele, C. H. Back, and M. R. Scheinfein, Phys. Rev. B **74**, 134404 (2006).

²C. D. Stanciu, A. V. Kimel, F. Hansteen, A. Tsukamoto, A. Itoh, A. Kirilyuk, and T. Rasing, Phys. Rev. B **73**, 220402 (2006).

³C. D. Stanciu, A. Tsukamoto, A. V. Kimel, F. Hansteen, A. Kirilyuk, A. Itoh, and T. Rasing, Phys. Rev. Lett. **99**, 217204 (2007).

⁴K.-J. Kim, S. K. Kim, Y. Hirata, S.-H. Oh, T. Tono, D.-H. Kim, T. Okuno, W. S. Ham, S. Kim, G. Go, *et al.*, Nat. Mater. **16**, 1187 (2017).

⁵M. Imai, Y. Ogata, H. Chudo, M. Ono, K. Harii, M. Matsuo, Y. Ohnuma, S. Maekawa, and E. Saitoh, Appl. Phys. Lett. **113**, 052402 (2018).

- ⁶S. J. Barnett, *Phys. Rev.* **6**, 239 (1915).
- ⁷S. J. Barnett, *Rev. Mod. Phys.* **7**, 129 (1935).
- ⁸C. G. de Oliveira and J. Tiomno, *Il Nuovo Cimento (1955-1965)* **24**, 672 (1962).
- ⁹M. Ono, H. Chudo, K. Harii, S. Okayasu, M. Matsuo, J. Ieda, R. Takahashi, S. Maekawa, and E. Saitoh, *Phys. Rev. B* **92**, 174424 (2015).
- ¹⁰Y. Ogata, H. Chudo, M. Ono, K. Harii, M. Matsuo, S. Maekawa, and E. Saitoh, *Appl. Phys. Lett.* **110**, 072409 (2017).
- ¹¹Y. Ogata, H. Chudo, B. Gu, N. Kobayashi, M. Ono, K. Harii, M. Matsuo, E. Saitoh, and S. Maekawa, *J. Magn. Magn. Mater.* **442**, 329 (2017).